Check for updates

Engineering high-brightness and long-lived organic room-temperature phosphorescence *via* systematic molecular design†

Guangming Wang,‡[a] Yuanyuan Chen,‡[ab] Xuefeng Chen,‡[a] Jinqi Zha,*[c] Xiaoya Guo*[b] and Kaka Zhang [ID] *[a]

We report a systematic molecular design in BF$_2$bdk-based afterglow emitters with photoluminescence quantum yields up to 46.3% and lifetimes around 1 s. Suitable excited-state types, diverse excited state species, relatively small singlet−triplet energy gaps and strong dipole−dipole interactions are critical in determining the afterglow properties.

Organic photofunctional materials exhibit wide application in diverse fields such as optical analysis, light harvesting, cosmetics, textile printing and dyeing.[1] Among them, organic room-temperature phosphorescence (RTP) and afterglow materials, characterized by their long-lived emission post-excitation source removal, hold significant promise for advanced anti-counterfeiting, bioimaging, and oxygen/microenvironment probing applications.[2] Among these, high-brightness organic afterglow materials, particularly those with phosphorescence lifetimes exceeding 100 ms, are especially noteworthy due to their easily detectable afterglow phenomena, even by the naked eye or low-cost equipment.[3] This makes them ideal for high-contrast biological monitoring, high-sensitivity analytical detection, information encryption and authentication, and organic optoelectronic devices.[4] The afterglow brightness $L(t)$ of organic afterglow materials at time t can be described by the equation $L(t) \sim \varepsilon^{\star} \Phi^{\star} \exp(-t/\tau)$, where ε is the molar absorption coefficients, Φ is the quantum efficiency, and τ is afterglow lifetime.[5] Hence, achieving high-brightness organic afterglow materials necessitates not only a large ε but also a high Φ and a long τ. However, in organic systems, triplet excited states are difficult to form due to spin–forbidden transitions and weak spin–orbit coupling, and they are easily deactivated at room temperature or body temperature, making the attainment of bright and long-lived organic room-temperature afterglow materials challenging.

To circumvent these limitations, researchers have employed strategies such as promoting intersystem crossing (ISC) through n–π⋆ transitions[6] and heavy atom effects (HAE),[7] protecting triplets in crystalline or glassy environments,[7,8] and other molecular design and material engineering strategies,[9] leading to the development of over a thousand examples of organic afterglow materials (Fig. S1, ESI†). Fig. S1 (ESI†) summarizes the performance metrics of organic afterglow materials in recent years, highlighting that efficient and long-lived organic afterglow materials with quantum efficiencies above 40% and lifetimes over 1 s still remain scarce (below 1% of the total organic afterglow materials). This scarcity stems from the fact that the introduction of HAE or n–π⋆ transitions in conventional molecular designs, while increasing the phosphorescence quantum yield (Φ_{P}), also tends to increase both the intersystem crossing rate (k_{ISC}) and the phosphorescence rate (k_{P}), resulting in shorter phosphorescence lifetimes (τ_{P}). Thus, selectively enhancing k_{ISC} to elevate Φ_{P}, while maintaining a low k_{P}, and simultaneously suppressing non-radiative (k_{nr}) and quenching (k_{q}) rates, is paramount for achieving high-efficiency long-lived phosphorescence.

We envision that by designing and synthesizing organic luminescent molecules with high ε, high k_{ISC} and low k_{P}, and subsequently doping them into suitable organic matrices, it is possible to achieve bright and long-lived organic afterglow materials. This material design strategy, on the one hand, can take advantage of the rigid and protective environment provided by the organic matrix to suppress k_{nr} and k_{q} of the luminescent molecules. Simultaneously, the dipole–dipole interactions between the organic matrix and the luminescent

[a] State Key Laboratory of Organometallic Chemistry and Shanghai-Hong Kong Joint Laboratory in Chemical Synthesis, Key Laboratory of Synthetic and Self-Assembly Chemistry for Organic Functional Molecules, Ningbo Zhongke Creation Center of New Materials, Shanghai Institute of Organic Chemistry, University of Chinese Academy of Sciences, Chinese Academy of Sciences, 345 Lingling Road, Shanghai 200032, People's Republic of China. E-mail: zhangkaka@sioc.ac.cn

[b] Department of Chemical Engineering, Shanghai University, Shanghai, 200444, China. E-mail: gxy@shu.edu.cn

[c] Ingenuity Biotechnology (Shanghai) Co., Ltd, 9th Floor, Block B, Building 1, No. 955 Liuxiang Road, Nanxiang Town, Jiading District, Shanghai 201802, People's Republic of China. E-mail: check.zha@ingenuitybio.com

† Electronic supplementary information (ESI) available: Experimental procedures, spectroscopic data. CCDC 2226200. For ESI and crystallographic data in CIF or other electronic format see DOI: https://doi.org/10.1039/d4cp02927e

‡ Equal contribution.

molecules can facilitate ISC process, leading to a high k_{ISC}, thereby realizing materials with enhanced efficiency and longevity.
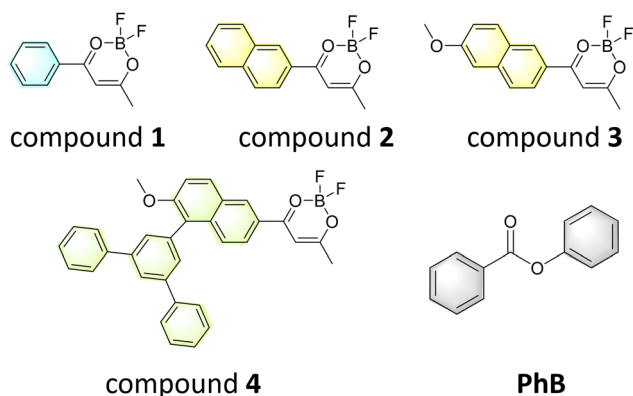
Difluoroboron β-diketonate (**BF$_2$bdk**) molecules, due to their large ε and high Φ, have been proven to be an excellent precursor for high-performance organic afterglow in previous studies by our group and others.[10] Moreover, **BF$_2$bdk** molecules possess significant dipole moments in their S_1 excited states, enabling strong dipole–dipole interactions with an organic matrix having a large ground-state dipole moment, which can promote their ISC and obtain a large k_{ISC}. Besides, phenyl benzoate (**PhB**) has been proved to be an ideal organic matrix for **BF$_2$bdk** molecules, due to its large ground-state dipole moment, as well as its rigid and protective environment. Therefore, in this work, we designed and synthesized a series of **BF$_2$bdk** molecules as efficient luminescent components, and doped them into **PhB** to prepare bright and long-lived two-component afterglow materials. By modulating the structure of the **BF$_2$bdk** molecules and manipulating their afterglow performance, bright and long-lived organic room-temperature afterglow materials with high quantum efficiencies of up to 46.3% and afterglow lifetimes of 976 ms have been achieved successfully. Further investigations reveal that suitable types of excited state transitions, diverse excited state species, relatively small singlet–triplet energy gaps ($\Delta E_{ST} \sim$ 0.3–0.4 eV), and strong dipole–dipole interactions all favour ISC and the emission of bright persistent luminescence, providing new insights and directions for the development of high-brightness, long-lived organic afterglow systems. These bright and long-lived organic afterglow materials also demonstrate promising applications in advanced anti-counterfeiting and information encryption.

Scheme 1 illustrates the chemical structures of the **BF$_2$bdk** molecules and the **PhB** matrix employed in this work, with the synthesis of the **BF$_2$bdk** molecules achieved *via* the cascade reaction developed by our group.[10] Comprehensive structural characterization has been performed on the synthesized **BF$_2$bdk** compounds, and their high purity can be confirmed through HPLC measurements following multiple recrystallizations using spectroscopic-grade dichloromethane/hexane (Fig. S2, ESI†). Table S1 (ESI†) summarizes the photophysical

Scheme 1 Chemical structures of **BF$_2$bdk** and **PhB** matrix.

properties of these **BF$_2$bdk** compounds in different solvents, showing their large ε, which attest to their superior photophysical properties and potential for intense luminescence (Fig. S3, ESI†). For example, compound **4** in dichloromethane solution exhibits a strong UV-vis absorption maximum at 380 nm ($\varepsilon = 4.07 \times 10^4\ M^{-1}\ cm^{-1}$) and an intense fluorescence emission at 462 nm with PLQY of 48.6%. The absorption band at 325–425 nm coincides well with the S_0–S_1 ICT transition as revealed by TD-DFT calculation and can be assigned to be ICT transition from the the aromatic donor to the dioxaborine acceptor (Fig. S4, ESI†). Besides, compounds **2** to **4** show positive solvatochromicity (Fig. S3, ESI†), which is consistent with the intramolecular charge transfer (ICT) nature in their S_1 states (Fig. S4–S6, ESI†). Compound **1** of localized excitation (LE) character in its S_1 state show similar fluorescence maxima in different solvents (Fig. S3 and S7, ESI†).

No noticeable afterglow can be observed from either solution-state or solid-powder-state **BF$_2$bdk** compounds at room temperature (Fig. S8, ESI†). In the powder and crystal states of **BF$_2$bdk**, molecular aggregation of **BF$_2$bdk** can cause afterglow quenching in the organic systems. **PhB** matrix can disperse luminescent dopants and prevent afterglow quenching caused by the electronic coupling of **BF$_2$bdk** aggregates. On the other hand, the dipole–dipole interaction between ground-state **PhB** and **BF$_2$bdk**'s S_1 state can enhance ISC of the organic system. Therefore, **PhB** matrix is introduced to obtain **BF$_2$bdk-PhB** materials with room-temperature afterglow property (Text S1, ESI†). When compound **1** was doped into **PhB** at a concentration of 0.01 wt%, the resultant 0.01%-**1-PhB** materials exhibit a weak green afterglow lasting approximately 5 s at room temperature (Fig. 1A), with a maximum emission peak at 485 nm and afterglow lifetime of 412 ms (Fig. 1C and E). This afterglow emission, which has already been confirmed to originate from the T_1 emission of compound **1** in our group's previous work,[10c] is an RTP-type afterglow emission. The steady-state emission spectrum of 0.01%-**1-PhB** afterglow materials exhibits a maximum emission peak at 390 nm, from which S_1 level can be estimated to be 3.18 eV (Fig. 1C). At 77 K, the phosphorescence peak of 0.01%-**1-PhB** afterglow materials is at 495 nm, closely matching the room-temperature value, from which we can estimate the T_1 energy level to be 2.51 eV (Fig. S9, ESI†). The room-temperature photoluminescence quantum yield (PLQY) value of 0.01%-**1-PhB** was measured to be as low as 0.43%, consistent with the low PLQY value of its solution. Unlike the **BF$_2$bdk**-matrix afterglow materials in our previous work where the **BF$_2$bdk**'s S_1 states have ICT character,[10] because a single benzene ring has limited electron-donating strength, compound **1** shows prominent LE character in its S_1 state as revealed by TD-DFT calculation (Fig. 1F). It is known that LE system usually has large singlet–triplet splitting energy (ΔE_{ST}); here 1-**PhB** sample has ΔE_{ST} value of 0.67 eV as estimated from its fluorescence and phosphorescence maxima (Fig. 1C). Because of the large ΔE_{ST}, 1-**PhB** system has limited ISC and thus weak RTP (Fig. 1A).

To enhance luminescence efficiency and afterglow brightness of **BF$_2$bdk-PhB** materials, a naphthyl substituent group,

This journal is © the Owner Societies 2024

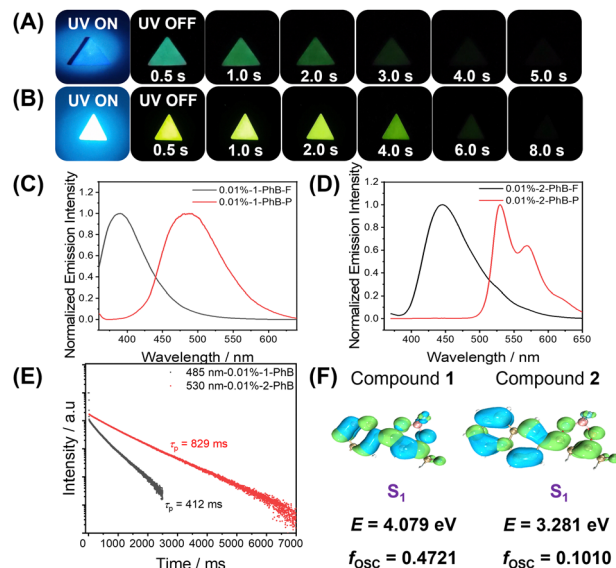*Phys. Chem. Chem. Phys.*, 2024, **26**, 24774–24778 | **24775**

Fig. 1 (A) and (B) Photographs of **1**-**PhB** (A) and **2**-**PhB** (B) materials. (C) and (D) Steady-state and delayed emission spectra of **1**-**PhB** (C) and **2**-**PhB** (D) excited at 365 nm. (E) Delayed emission profiles of **1**-**PhB** and **2**-**PhB** monitored at 485 nm and 530 nm. (F) TD-DFT calculation of **1**'s and **2**'s S$_1$ states.
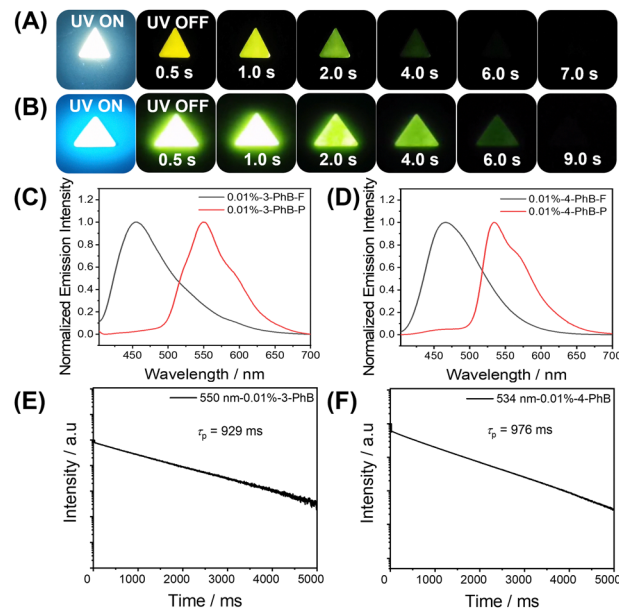

Fig. 2 (A) and (B) Photographs of **3**-**PhB** (A) and **4**-**PhB** (B) materials. (C) and (D) Steady-state and delayed emission spectra of **3**-**PhB** (C) and **4**-**PhB** (D) excited at 365 nm. (E) and (F) Emission decay profiles of **3**-**PhB** (E) and **4**-**PhB** (F) monitored at 550 nm and 534 nm.

known for its greater ISC capability than phenyl, is further introduced to obtain compound **2**.[10b] The resultant 0.01%-**2**-**PhB** materials display bright blue fluorescence at room temperature, with a significantly increased PLQY of 26.1% (Fig. 1B). In a dark room, **2**-**PhB** materials can exhibit a bright yellow-green afterglow (Fig. 1B), which has been previously established to be RTP-type afterglow originating from **2**'s T$_1$ emission.[10g] The steady-state and delayed emission spectra of the **2**-**PhB** materials reveal a fluorescence maximum at 442 nm (S$_1$ = 2.81 eV), a phosphorescence peak at 529 nm (T$_1$ = 2.34 eV) with phosphorescence lifetime of 829 ms (Fig. 1D and E). These results indicate a marked improvement in both afterglow brightness and lifetime of **2**-**PhB** compared to **1**-**PhB**. This enhancement aligns with theoretical calculated results. TD-DFT calculation demonstrates that **2**'s S$_1$ states exhibit a pronounced ICT nature, distinctly different from the LE characteristics of **1** (Fig. 1F). Moreover, ΔE_{ST} of **2**-**PhB** materials can be estimated to be 0.47 eV, which would facilitate ISC to a certain extent and favor efficient phosphorescence emission.

Further enhancement of the PLQY is achieved by introducing an electron-donating methoxy group into compound **2**, resulting in 0.01%-**3**-**PhB** materials with PLQY of 39.11%. At room temperature, **3**-**PhB** materials display a bright blue fluorescence, and a yellow RTP-type afterglow (Text S2 and S3, ESI†) lasting for 7 s (Fig. 2A). The steady-state emission spectrum of **3**-**PhB** materials shows a fluorescence band at 455 nm (Fig. 2B, S$_1$ = 2.73 eV), while their delayed emission spectrum shows a phosphorescence peak at 550 nm (T$_1$ = 2.25 eV) with lifetime of 929 ms (Fig. 2C and E). TD-DFT calculation shows that, the sum of the SOCMEs between the triplet excited states (T$_n$, n = 1–3) and S$_1$ in **3**, denoted as SOCME(sum) = SOCME(T$_1$–S$_1$) + SOCME(T$_2$–S$_1$) + SOCME(T$_3$–S$_1$), increases significantly

from 0.88 to 1.16 cm^{-1}, suggesting a notable improvement in ISC ability (Fig. S5 and S6, ESI†). The enhancement in SOCME contribute to the strengthened afterglow brightness of **3**-**PhB** compared to **2**-**PhB**. The estimated ΔE_{ST} of **3**-**PhB** materials is 0.48 eV, similar to that of **2**-**PhB** materials, indicating that the introduction of the methoxy group has little effect on ΔE_{ST} in this system.

Twisted donor units, as demonstrated in our and others' previous work, can reduce ΔE_{ST}, promoting ISC and efficient afterglow emission.[10a,d,f] Inspired by this, a twisted polycyclic aromatic unit is further introduced into **3** to obtain **4**. The resultant 0.01%-**4**-**PhB** materials still exhibit a bright blue fluorescence at room temperature with PLQY as high as 46.3% (Fig. 2B), and their steady-state emission spectrum features a fluorescence peak at 467 nm (Fig. 2D, S$_1$ = 2.66 eV). In a dark room, **4**-**PhB** materials can exhibit a very bright yellow-green RTP-type afterglow (Text S2 and S3, ESI†) lasting approximately 9 s (Fig. 2B), with a phosphorescence band at 534 nm (Fig. 2D, T$_1$ = 2.32 eV) in their delayed emission spectrum and lifetime of 976 ms (Fig. 2F). **4**-**PhB** materials can also exhibit significant afterglow at 77 K with a similar phosphorescence peak at 550 nm (Fig. S10, ESI†). The estimated ΔE_{ST} of **4**-**PhB** afterglow materials is 0.34 eV, notably lower than that of other **BF$_2$bdk**-**PhB** materials. Furthermore, TD-DFT calculation indicates that, besides S$_1$-to-T$_1$ ISC channel, S$_1$-to-T$_n$ (n = 2 or 3) channels are responsible for the population of T$_1$ states in **BF$_2$bdk** systems; the S$_1$–T$_n$ energy gap is smaller than that of S$_1$–T$_1$. Besides, compared to **2** and **3**, **4** exhibits more distinct differences in the excited states between T$_n$ (n = 1–3) and S$_1$ states, along with larger SOCME$_{T_n-S_1}$ values, particularly SOCME$_{T_1-S_1}$ = 0.46 cm^{-1} (Fig. S4, ESI†). According to the energy gap

law and the EI-Sayed rule, such differences in excited states and larger $SOCME_{T_n-S_1}$ values can significantly facilitate the formation of multiple ISC pathways between T_n and S_1 states, promoting ISC process and efficient phosphorescence.

Similarly, TD-DFT calculation also reveals that the S_1 dipole moments of the **BF₂bdk** molecules follow the order **4** > **3** > **2** > **1** (Table S2, ESI†). **PhB** matrix, which has a ground-state dipole moment of 1.94 D, can interact with **BF₂bdk**'s S_1 excited state *via* dipole–dipole interaction (with less influence on **BF₂bdk**'s T_1 energy levels), lower **BF₂bdk**'s S_1 energy levels and thus narrow ΔE_{ST} to enhance intersystem crossing.[10e–h] Thus, a larger S_1 dipole moment of the luminescent molecules leads to stronger dipole–dipole interactions with the matrix, favoring the enhancement of ISC process as well as the afterglow performance of **BF₂bdk-PhB** materials.[10e,g] Besides, we select cyclo olefin polymer (COP), poly(methyl methacrylate) (PMMA), **PhB** and 4-methoxybenzophenone (MeOBP) to serve as organic matrix to prepare **BF₂bdk**-matrix samples. Corresponding steady-state and delayed emission spectra, as well as fluorescence decay profiles, have been collected (Fig. S11–S14 and Table S3 and S4, ESI†). The emission studies show that **BF₂bdk**'s S_1 energy levels decrease with the dipole moments of organic matrices while **BF₂bdk**'s T_1 energy levels have insignificant change. Overall, **BF₂bdk** molecules in organic matrices with large dipole moments have small ΔE_{ST} and strong tendency of intersystem crossing. The fluorescence lifetimes of **BF₂bdk**'s S_1 states have been found first increase with dipole moments from COP through PMMA to **PhB** and then decrease from **PhB** to MeOBP. The lifetime increase is attributed to the decrease of **BF₂bdk**'s fluorescence decay rates in polar environment as supported by the reported studies, while the significant increase of intersystem crossing from **PhB** to MeOBP should be responsible for the lifetime decrease. These results reveal the effect of dipole–dipole interaction between ground-state matrix and S_1-state **BF₂bdk** for the enhancement of intersystem crossing of the **BF₂bdk**-matrix system, which has also been supported by our previous study and the reported studies.[10e,g]

In summary, appropriate types of excited state transitions, a rich diversity of excited states, relatively small ΔE_{ST} (0.3–0.4 eV), and strong dipole–dipole interactions are the reasons behind the superior afterglow brightness and PLQY of **4-PhB** materials compared to **3-PhB** > **2-PhB** > **1-PhB**.

Notably, the afterglow colors of these **BF₂bdk-PhB** materials were distinctly red-shifted relative to their fluorescence colors, with the afterglow peaks being red-shifted relative to the fluorescence peaks. This suggests that their afterglow emissions belong to organic room-temperature phosphorescence. The phosphorescence emissions of **1-PhB** and **2-PhB** materials were previously attributed to the T_1 emission of the **BF₂bdk**, and the same should hold true for the persistent emissions of **3-PhB** and **4-PhB** materials.

In the field of information encryption and anti-counterfeiting technologies, fluorescence inks have gained widespread use due to their excellent printability and high-resolution features.[4e,f] However, their ease of replication limits their application in scenarios requiring higher security levels.
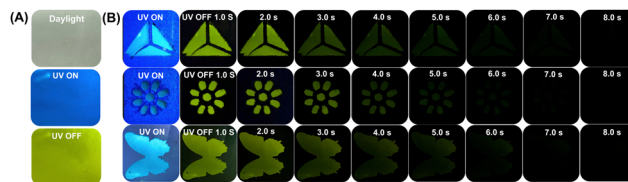

Fig. 3 (A) Photographs of **4-PhB** afterglow plates (20 cm × 20 cm) at different conditions. (B) Photographs of **4-PhB** afterglow plates behind different pre-designed masks.

Organic room-temperature afterglow materials, with their unique long-lived excited state properties enabling time-resolved multiplexed information encryption, show vast potential for advanced anti-counterfeiting and information encryption applications. **PhB** matrix, with its low melting point (70 °C), endows **BF₂bdk-PhB** afterglow materials with outstanding processability, allowing them to be fabricated into afterglow plate, as well as various persistent afterglow patterns (Fig. 3A and B). These **BF₂bdk-PhB** afterglow plates appear as inconspicuous white glass plates under daylight but exhibit intense blue fluorescence under a 365 nm lamp (Fig. 3A). After removing the lamp, they can display bright yellow-green afterglow. Moreover, when using different pre-designed masks, these afterglow plates can exhibit yellow-green afterglow with different patterns after the excitation source is removed, demonstrating potential applications in the display sector (Fig. 3B).

In conclusion, through systematic molecular design and strategic incorporation into protective organic matrices, we have successfully developed a series of high-brightness and long-lived organic room-temperature afterglow materials. By modulating the structure of the **BF₂bdk** molecules and manipulating their afterglow performance, achieving afterglow materials with PLQY > 40% and afterglow lifetime around 1 s. Our findings underscore the significance of suitable excited state transitions, diverse excited state species, small singlet–triplet energy gaps, and strong dipole–dipole interactions in the realization of high-performance afterglow materials. These materials not only advance the fundamental understanding of organic room-temperature afterglow materials but also open up new avenues for their practical applications in advanced anti-counterfeiting, information encryption, and display technologies.

Data availability

The data supporting this article have been included as part of the ESI.†

Conflicts of interest

There are no conflicts to declare.

Acknowledgements

This journal is © the Owner Societies 2024

Phys. Chem. Chem. Phys., 2024, **26**, 24774–24778 | **24777**

Notes and references

1 (a) V. W.-W. Yam, V. K.-M. Au and S. Y.-L. Leung, *Chem. Rev.*, 2015, **115**, 7589–7728; (b) Y. Hong, J. W. Y. Lam and B. Z. Tang, *Chem. Soc. Rev.*, 2011, **40**, 5361; (c) J. Mei, N. L. C. Leung, R. T. K. Kwok, J. W. Y. Lam and B. Z. Tang, *Chem. Rev.*, 2015, **115**, 11718–11940; (d) H. Zhou, Y. Zhang, C.-K. Mai, S. D. Collins, T.-Q. Nguyen, G. C. Bazan and A. J. Heeger, *Adv. Mater.*, 2014, **26**, 780–785; (e) K. Y. Zhang, Q. Yu, H. Wei, S. Liu, Q. Zhao and W. Huang, *Chem. Rev.*, 2018, **118**, 1770–1839; (f) W. Zhang, J. Yao and Y. S. Zhao, *Acc. Chem. Res.*, 2016, **49**, 1691–1700; (g) W. L. Jorgensen, *Acc. Chem. Res.*, 2009, **42**, 724–733; (h) L.-K. Li, M.-C. Tang, S.-L. Lai, M. Ng, W.-K. Kwok, M.-Y. Chan and V. W.-W. Yam, *Nat. Photonics*, 2019, **13**, 185–191; (i) H. Uoyama, K. Goushi, K. Shizu, H. Nomura and C. Adachi, *Nature*, 2012, **492**, 234–238; (j) M. A. Baldo, D. F. O'Brien, Y. You, A. Shoustikov, S. Sibley, M. E. Thompson and S. R. Forrest, *Nature*, 1998, **395**, 151–154.

2 (a) W. Zhao, Z. He and B. Z. Tang, *Nat. Rev. Mater.*, 2020, **5**, 869–885; (b) S. Xu, R. Chen, C. Zheng and W. Huang, *Adv. Mater.*, 2016, **28**, 9920–9940; (c) S. Hirata, *Adv. Opt. Mater.*, 2017, **5**, 1700116; (d) N. Gan, H. Shi, Z. An and W. Huang, *Adv. Funct. Mater.*, 2018, **28**, 1802657; (e) X. Ma, J. Wang and H. Tian, *Acc. Chem. Res.*, 2019, **52**, 738–748; (f) Kenry, C. Chen and B. Liu, *Nat. Commun.*, 2019, **10**, 2111; (g) Q. Li and Z. Li, *Acc. Chem. Res.*, 2020, **53**, 962–973; (h) M. Singh, K. Liu, S. Qu, H. Ma, H. Shi, Z. An and W. Huang, *Adv. Opt. Mater.*, 2021, **9**, 2002197; (i) S. Guo, W. Dai, X. Chen, Y. Lei, J. Shi, B. Tong, Z. Cai and Y. Dong, *ACS Mater. Lett.*, 2021, **3**, 379–397; (j) H. Gao and X. Ma, *Aggregate*, 2021, **2**, e38; (k) X. Yan, H. Peng, Y. Xiang, J. Wang, L. Yu, Y. Tao, H. Li, W. Huang and R. Chen, *Small*, 2022, **18**, 2104073; (l) S. Hirata, *Appl. Phys. Rev.*, 2022, **9**, 011304; (m) L. Ma and X. Ma, *Sci. China: Chem.*, 2023, **66**, 304–314; (n) M. Ji and X. Ma, *Ind. Chem. Mater.*, 2023, **1**, 582–594; (o) H. Bhatia, I. Bhattacharjee and D. Ray, *J. Phys. Chem. Lett.*, 2018, **9**, 3808–3813; (p) H. Bhatia, S. Dey and D. Ray, *ACS Omega*, 2021, **6**, 3858–3865.

3 (a) J. Jin, H. Jiang, Q. Yang, L. Tang, Y. Tao, Y. Li, R. Chen, C. Zheng, Q. Fan, K. Y. Zhang, Q. Zhao and W. Huang, *Nat. Commun.*, 2020, **11**, 842; (b) X. Wang, Y. Sun, G. Wang, J. Li, X. Li and K. Zhang, *Angew. Chem., Int. Ed.*, 2021, **60**, 17138–17147.

4 (a) S. M. A. Fateminia, Z. Mao, S. Xu, Z. Yang, Z. Chi and B. Liu, *Angew. Chem., Int. Ed.*, 2017, **56**, 12160–12164; (b) X. Zhen, Y. Tao, Z. An, P. Chen, C. Xu, R. Chen, W. Huang and K. Pu, *Adv. Mater.*, 2017, **29**, 1606665; (c) C. A. DeRosa, S. A. Seaman, A. S. Mathew, C. M. Gorick, Z. Fan, J. N. Demas, S. M. Peirce and C. L. Fraser, *ACS Sens.*, 2016, **1**, 1366–1373; (d) W.-J. Guo, Y.-Z. Chen, C.-H. Tung and L.-Z. Wu, *CCS Chem.*, 2022, **4**, 1007–1015; (e) Y. Su, S. Z. F. Phua, Y. Li, X. Zhou, D. Jana, G. Liu, W. Q. Lim, W. K. Ong, C. Yang and Y. Zhao, *Sci. Adv.*, 2018, **4**, eaas9732; (f) Z. Xie, X. Zhang, H. Wang, C. Huang, H. Sun, M. Dong, L. Ji, Z. An, T. Yu and W. Huang, *Nat. Commun.*, 2021, **12**, 3522; (g) D. Wang, J. Gong, Y. Xiong, H. Wu, Z. Zhao, D. Wang and B. Z. Tang, *Adv. Funct. Mater.*, 2023, **33**, 2208895; (h) R. Kabe, N. Notsuka, K. Yoshida and C. Adachi, *Adv. Mater.*, 2016, **28**, 655–660.

5 (a) K.-L. Wong, J.-C. G. Bünzli and P. A. Tanner, *J. Lumin.*, 2020, **224**, 117256; (b) J. Li, W. Xia, J. Li, G. Wang, X. Wang, Z. Mo, X. Chen and K. Zhang, *Adv. Opt. Mater.*, 2023, **12**, 2302311.

6 (a) W. Z. Yuan, X. Y. Shen, H. Zhao, J. W. Y. Lam, L. Tang, P. Lu, C. Wang, Y. Liu, Z. Wang, Q. Zheng, J. Z. Sun, Y. Ma and B. Z. Tang, *J. Phys. Chem. C*, 2010, **114**, 6090–6099; (b) W. Zhao, Z. He, J. W. Y. Lam, Q. Peng, H. Ma, Z. Shuai, G. Bai, J. Hao and B. Z. Tang, *Chemistry*, 2016, **1**, 592–602.

7 O. Bolton, K. Lee, H.-J. Kim, K. Y. Lin and J. Kim, *Nat. Chem.*, 2011, **3**, 205–210.

8 S. Hirata, K. Totani, J. Zhang, T. Yamashita, H. Kaji, S. R. Marder, T. Watanabe and C. Adachi, *Adv. Funct. Mater.*, 2013, **23**, 3386–3397.

9 (a) D. Li, F. Lu, J. Wang, W. Hu, X.-M. Cao, X. Ma and H. Tian, *J. Am. Chem. Soc.*, 2018, **140**, 1916–1923; (b) X.-F. Wang, H. Xiao, P.-Z. Chen, Q.-Z. Yang, B. Chen, C.-H. Tung, Y.-Z. Chen and L.-Z. Wu, *J. Am. Chem. Soc.*, 2019, **141**, 5045–5050; (c) Z. Zhang, Y. Chen and Y. Liu, *Angew. Chem., Int. Ed.*, 2019, **58**, 6028–6032.

10 (a) Y. Sun, G. Wang, X. Li, B. Zhou and K. Zhang, *Adv. Opt. Mater.*, 2021, **9**, 2100353; (b) X. Li, G. Wang, J. Li, Y. Sun, X. Deng and K. Zhang, *ACS Appl. Mater. Interfaces*, 2022, **14**, 1587–1600; (c) J. Li, X. Wang, Y. Pan, Y. Sun, G. Wang and K. Zhang, *Chem. Commun.*, 2021, **57**, 8794–8797; (d) Y. Pan, J. Li, X. Wang, Y. Sun, J. Li, B. Wang and K. Zhang, *Adv. Funct. Mater.*, 2022, **32**, 2110207; (e) Y. Sun, J. Liu, J. Li, X. Li, X. Wang, G. Wang and K. Zhang, *Adv. Opt. Mater.*, 2022, **10**, 2101909; (f) G. Wang, X. Chen, J. Liu, S. Ding and K. Zhang, *Sci. China: Chem.*, 2023, **66**, 1120–1131; (g) B. Fu, G. Wang, J. Li, J. Li, X. Li, X. Zhao, S. Ding, G. Yan, Q. Yan and K. Zhang, *Chin. J. Chem.*, 2024, **42**, 1237–1246; (h) J. Li, X. Li, G. Wang, X. Wang, M. Wu, J. Liu and K. Zhang, *Nat. Commun.*, 2023, **14**, 1987.

24778 | *Phys. Chem. Chem. Phys.*, 2024, **26**, 24774–24778

This journal is © the Owner Societies 2024